A Path Planning Algorithm for UAV 3D Surface Inspection Based on Normal Vector Filtering and Integrated Viewpoint Evaluation
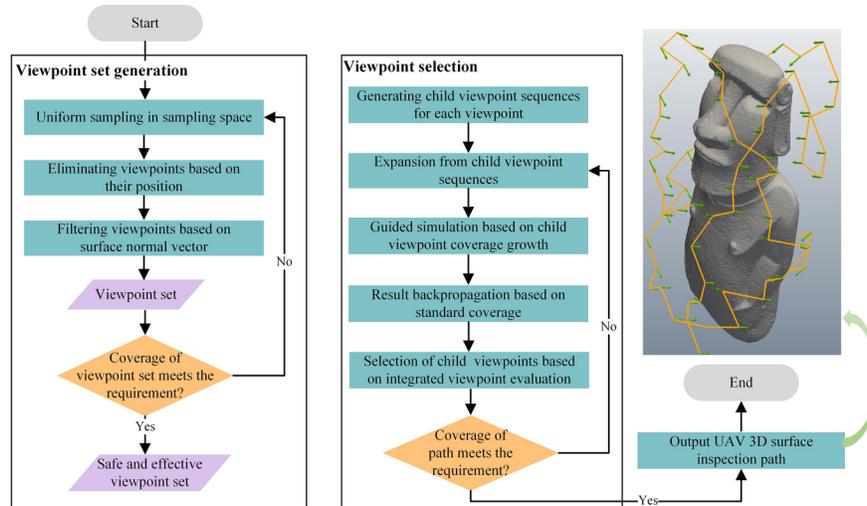
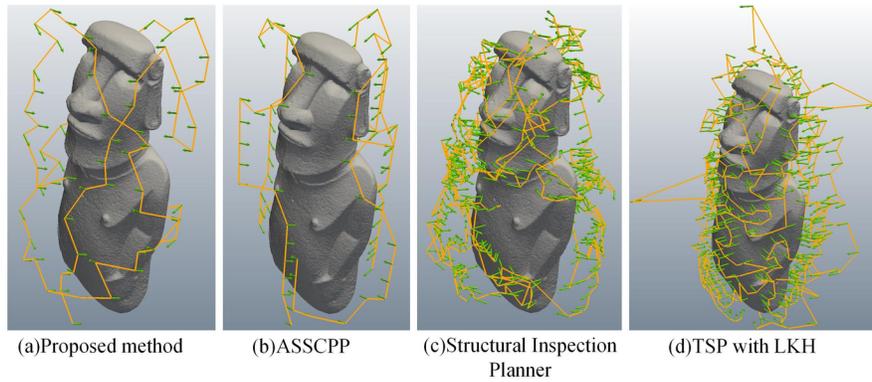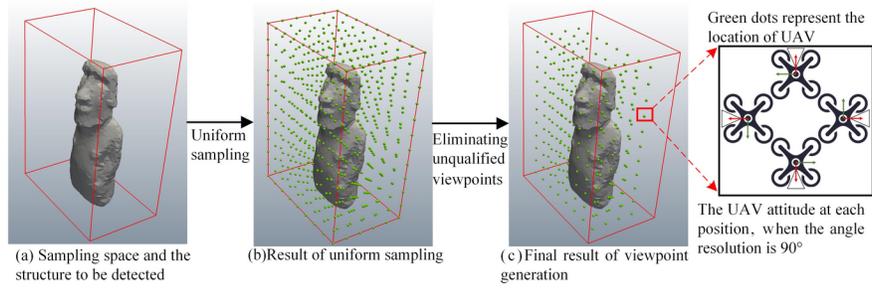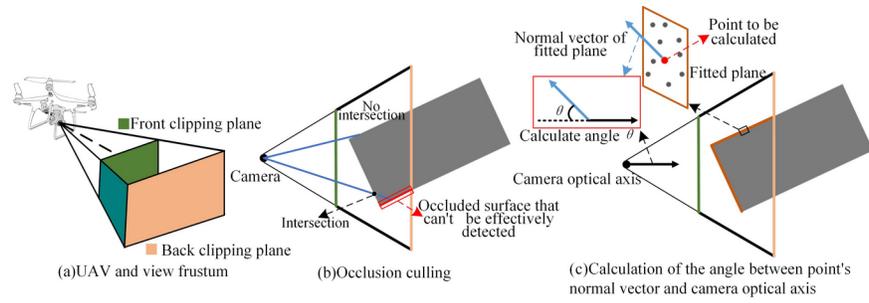Yunlong Wang[1], Shaoke Wan[1], Rongcan Qiu[1], and Xiaohu Li[1]

[1]Xi'an Jiaotong University Key Laboratory of Modern Design and Rotor-Bearing System
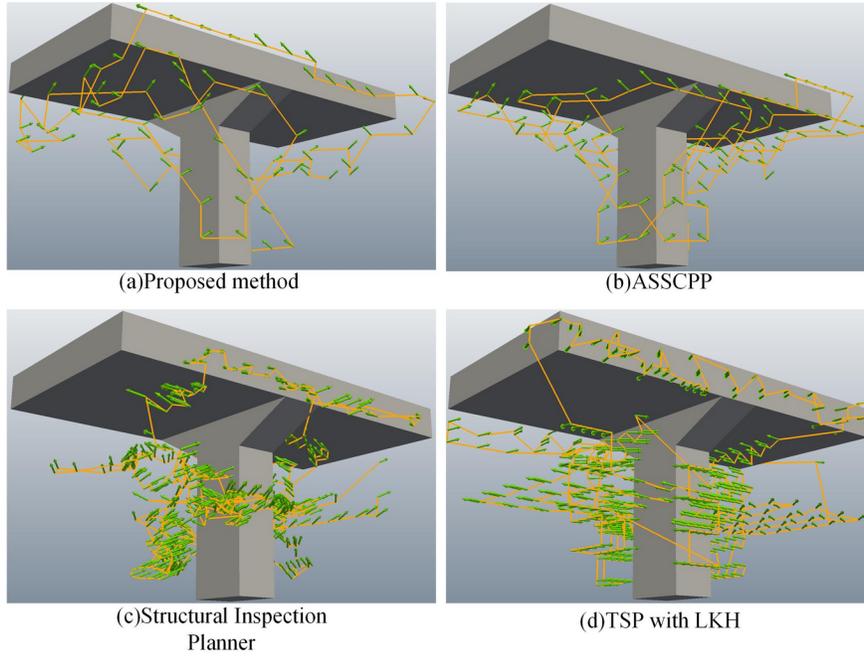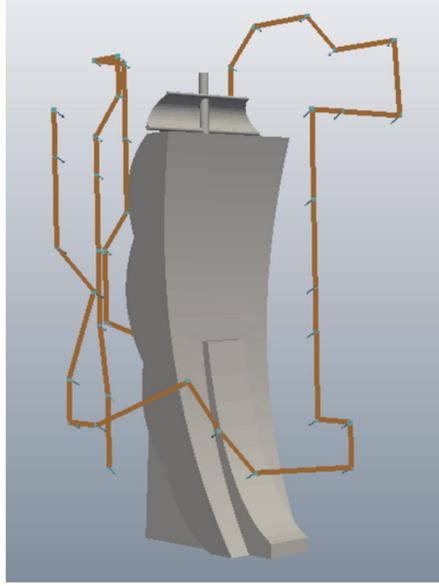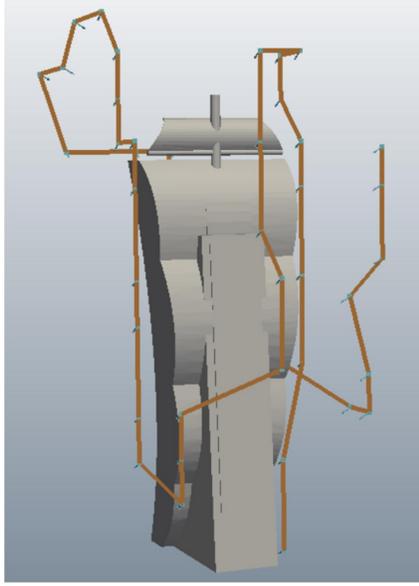
August 24, 2024

Abstract

The use of UAV for 3D surface inspection has become an important tool in the field of large-scale structure maintenance. However, the commonly used UAV inspection path planning algorithms for 3D surface suffer from problems such as path quality dependent model accuracy, path inspection efficiency, and low inspection quality. To address these issues, this paper proposes a UAV 3D surface inspection path planning algorithm based on normal vector filtering and integrated viewpoint Evaluation. Generate a safe and effective set of viewpoints through uniform sampling and normal vector viewpoint filtering, and then use a integrated viewpoint evaluation method combined with Monte Carlo tree search to select viewpoints, thereby generating a safe, efficient, and complete UAV surface inspection path. The results of simulation and physical experiments show that the proposed method can effectively solve the path planning problem when using UAV for surface inspection of large three-dimensional structures. Meanwhile, while ensuring the quality of inspection, this method can reduce path redundancy and improve the surface inspection efficiency of UAV.

Front clipping plane

Back clipping plane

(a)UAV and view frustum

No intersection

Camera

Intersection

Occluded surface that can't be effectively detected

(b)Occlusion culling

Normal vector of fitted plane

Point to be calculated

Fitted plane

Calculate angle θ

Camera optical axis

(c)Calculation of the angle between point's normal vector and camera optical axis

Uniform sampling

Eliminating unqualified viewpoints

(a) Sampling space and the structure to be detected

(b)Result of uniform sampling

(c)Final result of viewpoint generation

Green dots represent the location of UAV

The UAV attitude at each position, when the angle resolution is 90°

(a)Proposed method

(b)ASSCPP

(c)Structural Inspection Planner

(d)TSP with LKH

2

(a)Proposed method

(b)ASSCPP

(c)Structural Inspection Planner

(d)TSP with LKH

A Path Planning Algorithm for UAV 3D Surface Inspection Based on Normal Vector Filtering and Integrated Viewpoint Evaluation

Yunlong Wang[1,2] | **Shaoke Wan**[1,2] | **Rongcan Qiu**[1,2] | **Xiaohu Li**[1,2]

[1]Key Laboratory of Education Ministry for Modern Design & Rotor-Bearing System, Xi'an Jiaotong University, Xi'an, China

[2]School of Mechanical Engineering, Xi'an Jiaotong University, Xi'an, China

Correspondence

Corresponding author Xiaohu Li, No.28 Xianning West Road, Xi'an, Shaanxi 710049, P.R. China.
Email: li.xiaohu@xjtu.edu.cn

Abstract

The use of UAV for 3D surface inspection has become an important tool in the field of large-scale structure maintenance. However, the commonly used UAV inspection path planning algorithms for 3D surface suffer from problems such as path quality dependent model accuracy, path inspection efficiency, and low inspection quality. To address these issues, this paper proposes a UAV 3D surface inspection path planning algorithm based on normal vector filtering and integrated viewpoint Evaluation. Generate a safe and effective set of viewpoints through uniform sampling and normal vector viewpoint filtering, and then use a integrated viewpoint evaluation method combined with Monte Carlo tree search to select viewpoints, thereby generating a safe, efficient, and complete UAV surface inspection path. The results of simulation and physical experiments show that the proposed method can effectively solve the path planning problem when using UAV for surface inspection of large three-dimensional structures. Meanwhile, while ensuring the quality of inspection, this method can reduce path redundancy and improve the surface inspection efficiency of UAV.

KEYWORDS
UAV, Path planning, Surface inspection, Normal vector filtering, Integrated viewpoint evaluation

1 | FIRST LEVEL HEAD

With the rapid development of lcalization and navigation technology, there has been a significant increase in the application of unmanned aerial vehicle (UAV) for various tasks[1], such as ground traffic surveillance[2], wildfire tracking[3], smart farming[4,5], aerial goods delivery[6], environmental data collection[7], search-and-rescue missions[8], geological surveying[9], mobile wireless coverage[10,11], and structural surface inspection[12,13,14,15,16]. Large-scale 3D structure, such as bridges, large statue, and tall buildings, require regular inspection to ensure their integrity and safety. However, traditional inspection methods using manual or ground-based equipment are often time-consuming, labor-intensive, and potentially hazardous[17,18]. By leveraging the maneuverability and autonomy of UAVs, it becomes possible to efficiently inspect large-scale 3D structures in a rapid and cost-effective manner[19]. Furthermore, the use of 3D mapping and imaging techniques enables the collection of high-resolution data[20] for detailed analysis and decision-making[21]. The key challenge in realizing this vision lies in developing effective inspection path planning (IPP) algorithms for UAV[22,23].

The UAV surface inspection path planning algorithm essentially represents a model-based offline 3D coverage path planning (CPP) approach[24,25], wherein a comprehensive path plan is formulated through a pre-constructed model prior to the actual execution of the UAV's mission[24]. A pivotal shared objective of IPP algorithms is to ensure that the inspection sensors, typically passive optical sensors such as CCD cameras[26,27], are able to comprehensively cover the target 3D structural surface as the UAV traverses the planned path. The IPP algorithms aim to minimize the path length, thereby enhancing inspection efficiency, reducing energy consumption, and extending the operational duration of the UAV[28]. Beyond the comprehensiveness coverage and efficiency of the path, the inspection quality of the path is also of utmost importance[29]. To guarantee the accuracy of inspection results, it is imperative to thoroughly consider factors such as the effective inspection range of the sensors during the planning process. Moreover, the algorithms must be scalable to handle large-scale structures and capable of adapting to
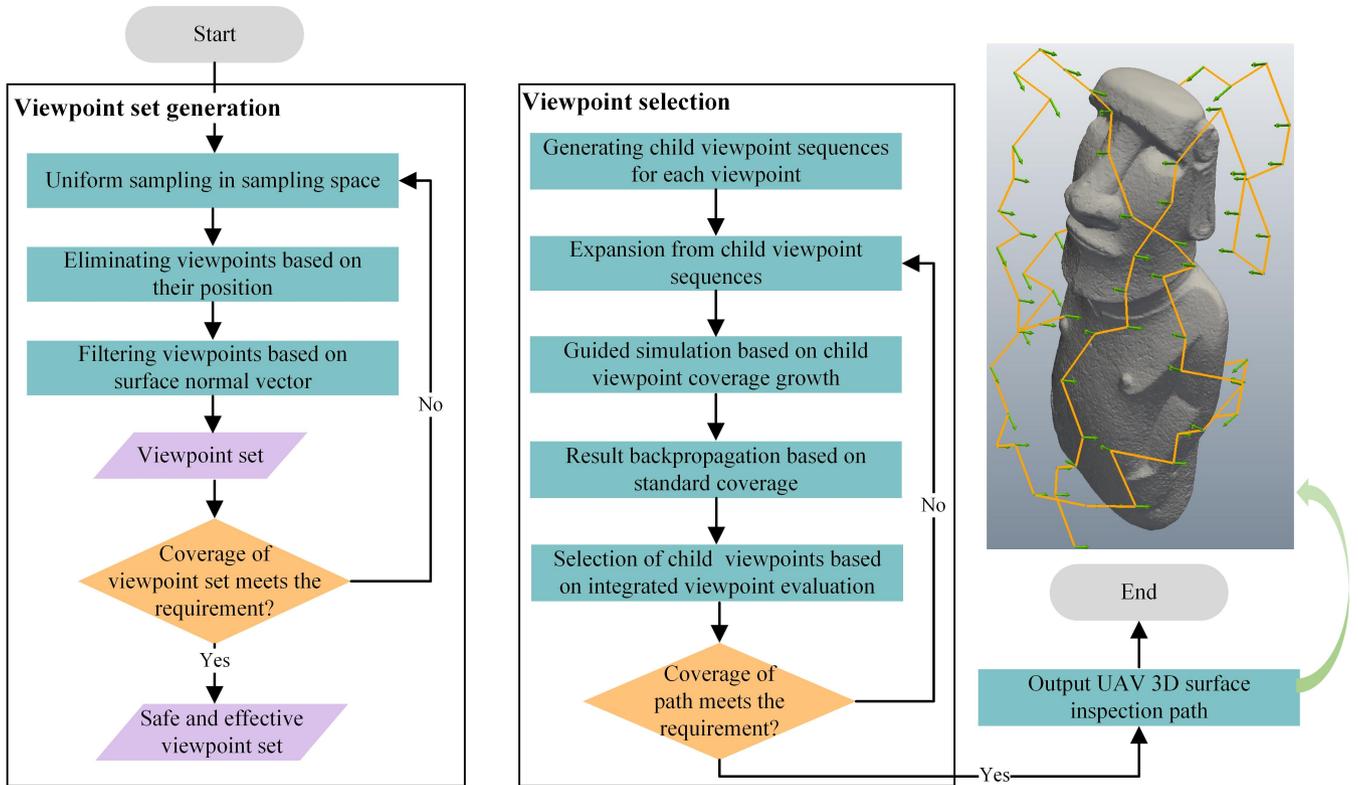
FIGURE 1 The flowchart of the proposed algorithm.

dynamic conditions such as structural variations. Given these application requirements,we are interested in designing a offline, model-based 3D coverage planning algorithm for structural inspection task with camera-quipped UAV.

In this paper, we propose a novel UAV large-scale 3D structural surface inspection path planning algorithm that incorporates normal vector filtering and integrated viewpoint evaluation.The main innovations and contributions of the study are as follows:

(1) The proposal of a viewpoint generation method based on normal vector filtering. Initially, a set of viewpoints is generated using uniform sampling to ensure completeness and safety for UAV surface inspection. Subsequently, an unqualified viewpoint filtering approach based on normal vectors is employed to eliminate inappropriate viewpoints, resulting in an accurate, effective, and quality-assured viewpoint set.

(2) The proposal of a viewpoint selection method that incorporates a integrated viewpoint evaluation framework with Monte Carlo Tree Search (MCTS). This approach effectively explores the viewpoint search space, preventing the algorithm from falling into local optima in large-scale 3D structure surface inspection path planning tasks. Simultaneously, it improves search efficiency and accuracy, ensuring that the selected viewpoints maximize path redundancy reduction while maintaining inspection quality.

(3) Extensive experimental validation has been conducted on the proposed UAV surface inspection path planning algorithm. Simulation results demonstrate that our proposed IPP algorithm achieves superior inspection efficiency and quality compared to alternative methods. Moreover, we have successfully implemented the proposed IPP algorithm on a UAV and validated its effectiveness in real-world scenarios.

The remainder of this paper is organized as follows. Section 2 introduces the related work. Section 3 describes the details of viewpoint generation method based on normal vector filtering. Section 4 provides the methodology for the viewpoint selection method that incorporates a integrated viewpoint evaluation framework with MCTS. To validate the practical applicability of the proposed 3D surface IPP algorithm for UAV, both simulation experiments and real-world UAV experiments were conducted and analysis are described in detail in Section 5. Finally, Section 6 concludes with remarks and future directions. The flowchart of the proposed algorithm is shown in Fig.1.

2 | RELATED WORK

In recent years, significant research efforts have been devoted to the development of surface IPP algorithms for UAV due to its importance for large-scale structure maintenance [30,31]. Current studies on surface IPP can be categorised into two groups,namely cell decomposition and viewpoint sampling [32].

The method based on cell decomposition is currently a well-established approach for UAV surface IPP. This technique divides the three-dimensional structure to be inspected into multiple simplified cells, tailored to the specific task and application requirements, and selects appropriate simple curves for each cell to achieve complete coverage [32].The key advantage of this method is its ability to break down complex IPP problems into smaller, more manageable subproblems, thereby enhancing the feasibility and efficiency of path planning. Choest et al. [33]pioneered the Boutropedon element decomposition method to achieve complete coverage path planning in two-dimensional planes; Building on this foundation, Acar et al. [34]proposed the Morse decomposition coverage algorithm combined with the Morse function to generate a three-dimensional complete coverage path. Li Yuanhong [32]segmented the overall bridge inspection path planning task into the complete coverage of bridge decks and bridge piers, accomplishing both sub-tasks through Morse decomposition and circular and linear trajectories. Peng et al. [35]proposed a hierarchical framework to extract building features, and subsequently obtained a three-dimensional surface inspection path utilizing a genetic algorithm. Jing et al. [24]used path primitives and primitive coverage maps to determine the coverage of each viewpoint, and then used greedy neighborhood search to minimize the distance of the path while meeting the requirements of UAV surface inspection. However, methods rooted in cell decomposition are usually tailored to specific three-dimensional structures, resulting in limited algorithmic generalizability. Furthermore, the utilization of fixed coverage curves restricts path flexibility [36], potentially leading to increased path length and decreased efficiency in the UAV's surface inspection process. The samplingbased methodology also finds extensive application in the realm of UAV surface inspection [37]. This approach typically encompasses two primary stages [38]. Initially, it involves random sampling within the designated target area or the generation of a discrete set of viewpoints employing specific methodologies. The process of generating these viewpoints is called view planning or viewpoint planning problem (VPP). Subsequently, through strategies aimed at minimizing path length or specific cost, the optimal viewpoints are selected and integrated into a UAV's inspection path. The sampling-based approach exhibits remarkable flexibility in adapting to diverse task requirements of 3D structures, thus rendering it highly efficient and feasible for large-scale 3D surface inspection tasks [24]. Englot et al. [39]pioneered the utilization of the Art Gallery Problem model as a framework for addressing the challenge of viewpoint generation in surface inspection path planning. This approach offers a novel perspective on the optimization of UAV-based surface inspection. Based on this framework, they subsequently transformed the process of viewpoint selection into the resolution of the Traveling Salesman Problem (TSP) [40], enabling the generation of a comprehensive inspection path. Since then, generating viewpoints by sampling and obtaining paths through the resolution of the TSP have emerged as the prevalent framework in the realm of sampling-based IPP. Bircher et al. [41]iteratively refined the viewpoints through resampling to enhance their quality and determined the optimal path connection method by addressing the TSP. The application of swarm intelligence methods in the field of IPP algorithms to solve TSP is also very extensive [15]. Neshat et al. [42]introduced a three-dimensional path planning approach for bridge inspection, which involved segmenting the underside of the bridge into smaller cells. This method generated viewpoints based on the scanning range of LiDAR sensors and employed genetic algorithm and A* algorithm to solve the TSP, thereby obtaining an optimal surface inspection path for UAVs. Shang et al. [15]utilizes a particle swarm optimization (PSO) framework which iteratively optimizes the paths without needing to discretize the motion space or simplify the sensing models as is done in similar methods. Other methods, such as search algorithms, are also commonly utilized in the viewpoint selection process of sampling-based IPP algorithms. Almandhou et al. [43,44,45]proposed an Adaptive Search Space Coverage Path Planning Algorithm (ASSCPP), which utilized an adaptive viewpoint generation technique to create a set of viewpoints. Subsequently, a graph search algorithm was employed to select the most suitable viewpoints. Dai Jiajia et al. [46]adopted a discrete three-dimensional grid map for generating viewpoints. Following this, an improved WaveFront algorithm was implemented to derive optimal paths for aircraft surface inspection using UAV. However, the sampling-based methods, due to the limitations of their viewpoint generation techniques, often require high-precision models, which readily result in redundant inspection paths. Furthermore, these sampling-based approaches tend to overlook the angle between the camera's optical axis and the surface to be inspected when generating viewpoints, leading to distorted information capture and difficulties in accurately accomplishing 3D structural surface inspection tasks. Large-scale 3D structural surfaces, in particular, necessitate an extensive array of viewpoints for comprehensive coverage, while also considering factors such as path length and inspection quality, posing significant challenges to viewpoint selection strategies.

3 | NORMAL VECTOR FILTERING-BASED VIEWPOINT SET GENERATION

The quintessence of the UAV surface inspection task lies in the comprehensive coverage of the target structure's surface by the sensor, with the inspection path adhering to stringent safety and quality standards. As previously stated, the UAV surface IPP methodology, which relies on viewpoint sampling, formulates paths by systematically selecting the optimal viewpoints. Consequently, the quality of the viewpoint set plays a pivotal role in determining the completeness and effectiveness of the inspection task. In the methodology presented in this paper, we ensure the completeness and security of inspection by uniformly sampling the sampling space to generate an initial viewpoint set. Furthermore, we refine this initial set by employing normal vector-based filtering, thereby enhancing inspection efficacy and reducing the search space, ultimately leading to a higher convergence rate for the algorithm. The details of proposed viewpoint set generation method are shown in Algorithm 1.

Algorithm 1 Normal vector filtering-based viewpoint set generation algorithm

---

Input: 1)Model of structure to be inspected, 2)position resolution r_p, 3)angular resolution r_a, 4) maximum inspection distance $d_{\max}$, 5) minimum safe distance $d_{\min}$, 6)normal vector filtering threshold θ_0.

Output: Accurate, effective, and quality-assured viewpoint set.

1: Generate initial viewpoints by uniformly sampling based on r_p and r_a (Eq.(2))
2: Eliminating viewpoints located inside the model
3: Eliminating viewpoints that are too close or too far from the model (Eq.(4))
4: **for** Each $VP_{ijkn} \in$ initial viewpoint set **do**
5:    **for** Each point p within the range of VP_{ijkn}'s frustum **do**
6:       **if** $N_{inter}(p) = 0$ **then**
7:          Add p to set P_{occ} (Eq.(5))
8:       **end if**
9:    **end for**
10:    **for** Each point $p_{occ} \in P_{occ}$ **do**
11:       **if** $\theta(p_{occ}) < \theta_0$ **then**
12:          Add p_{occ} to set P_{filter} (Eq.(13))
13:       **end if**
14:    **end for**
15:    **if** $S_{ijkn} < S_0$ **then**
16:       Filter VP_{ijkn} from initial viewpoint set(Eq.(14))
17:    **end if**
18: **end for**
    return Outputs

3.1 | Initial viewpoint set generation

To limit the sampling range and reduce computational complexity, it is necessary to set a sampling space containing the three-dimensional structure to be detected, and all viewpoints and drone detection paths will also be located in the sampling space, as shown in Fig.2(a). Therefore, there is a minimum constraint on the size of the sampling space to ensure effective viewpoint sampling and path planning:

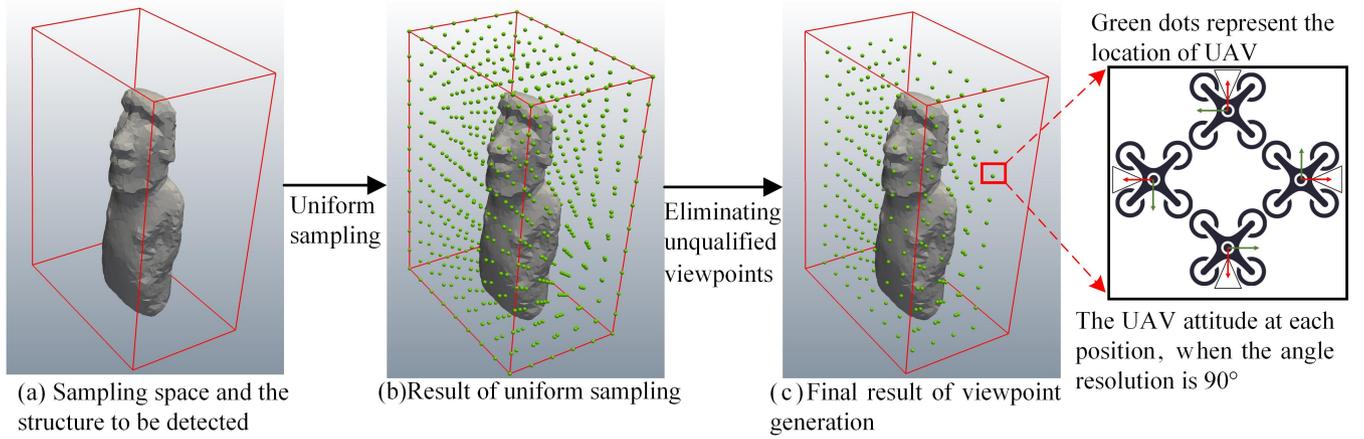$$\begin{cases} L \geq l + 2d_{\max} \\ H \geq h + 2d_{\max} \\ W \geq w + 2d_{\max} \end{cases} \tag{1}$$

(a) Sampling space and the structure to be detected

(b)Result of uniform sampling

(c) Final result of viewpoint generation

Green dots represent the location of UAV

The UAV attitude at each position, when the angle resolution is 90°

FIGURE 2 Sampling space and result of viewpoint generation.

where L, H, W are the length, width, and height of the sampling space; l, h, w represent the length, width, and height of the three-dimensional structure to be tested; $d_{\max}$ is the maximum inspection distance, determined by the effective inspection range of the inspection sensor.

The method proposed in this article generates initial viewpoint set that can fully cover the surface of the structure to be inspected by uniformly sampling the position coordinates and angles in the sampling space. Divide the sampling space into equally sized cubes with a certain resolution, and the vertices of each cube represent a possible position of the UAV's viewpoint. Next, samples are taken at each viewpoint position at a certain angular resolution to obtain viewpoints containing attitude information. This uniform sampling process ensures that the generated initial viewpoint set can uniformly and comprehensively cover the surface of the structure to be inspected, and contains sufficient angle information, as shown in Fig.2(b). The sampling formula is as follows:

$$VP_{ijkn} = (x_i, y_j, z_k, \psi_n)$$

$$\begin{cases} x_i = x_0 + i^* r_p \\ y_j = y_0 + j^* r_p \\ z_k = z_0 + k^* r_p \\ \psi_n = \psi_0 + n^* r_a \end{cases} , i,j,k \in \mathbb{N}^* \tag{2}$$

where VP_{ijkn} is the generated viewpoint; x_i, y_j, z_k, ψ_n represent the position and yaw angle of the UAV at this viewpoint; Cd is the starting point of the entire sampling space; r_p is the position resolution, which is generally determined by the detection range of the detection camera; r_a is the angular resolution.

The initial viewpoint set generated by the uniform sampling method are uniformly distributed in the sampling space, and the position and attitude distribution of the viewpoints are independent of factors such as the shape and detail size of the structure to be inspected. This attribute guarantees both the consistency of the viewpoint set and the comprehensiveness of the surface coverage for the structure under inspection. At the same time, this also ensures the universality of the UAV surface IPP algorithm proposed in this article, minimizing the influence of structure shape and model accuracy on the efficacy of path planning.

In the initial viewpoint set generated by uniform sampling, there exist viewpoints located inside the model or excessively close to or far from the model. To ensure the safety and effectiveness of the inspection process, it is necessary to eliminate these viewpoints from the set. In this process, viewpoints inside the model must be removed first to prevent the generation of ineffective paths. This step is achieved by calculating the number of intersections between the line segment formed by connecting the viewpoint and any point outside the model and the model itself. If the number of intersections is odd, the viewpoint is inside the model and needs to be eliminated; if the number of intersections is even, the viewpoint is outside the model. Therefore, the flag of the initial viewpoints can be modified based on the number of intersections as follows,

$$flag_{ijkn} = \begin{cases} 1, MOD(N_{inter}, 2) = 0 \\ 0, MOD(N_{inter}, 2) = 1 \end{cases} \tag{3}$$
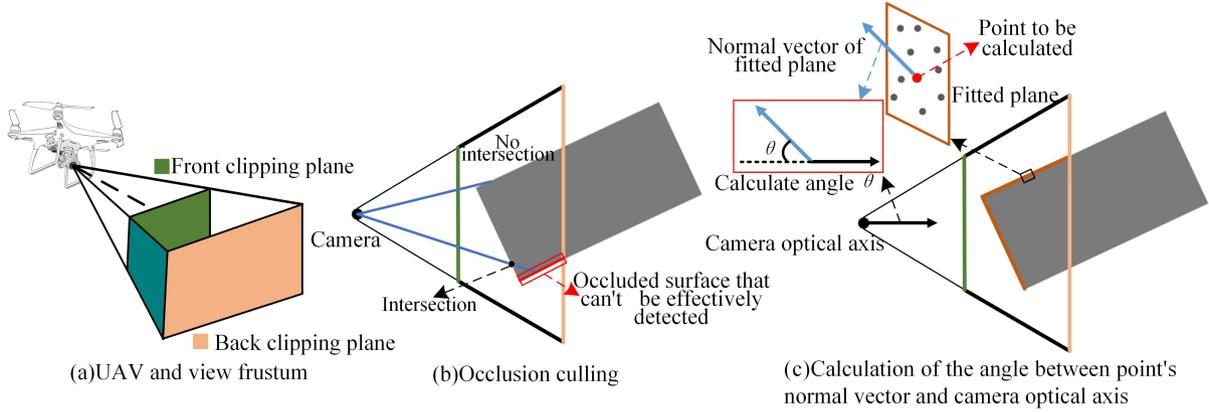
FIGURE 3 Sampling space and result of viewpoint generation.

where, $flag_{ijkn}$ represents the filtering flag of the viewpoint. If its value is 0, the viewpoint will be removed. If its value is 1, the viewpoint will be retained; N_{inter} is the number of intersection points between the line segment and the model.

Furthermore, it is crucial to eliminate the viewpoints in the initial set that are excessively close to or distant from the model, based on the UAV's safe distance and the camera's inspection range. This refinement aims to enhance the safety of the surface inspection task, preventing potential collisions between the drone and the model, thus averting potential damage. Additionally, it ensures the validity of the collected data, ultimately improving the accuracy of the inspection results. Specifically, this process can be described as follows:

$$flag_{ijkn} = \begin{cases} 1, d_{\min} \leq d_{ijkn} \leq d_{\max} \\ 0, d_{ijkn} \leq d_{\min} \text{or} d_{iijkn} \geq d_{\max} \end{cases} \qquad (4)$$

where $d_{\min}$ is the minimum safe distance between the UAV and the structure to be inspected; d_{ijkn} is the actual distance between the viewpoint and the structure to be inspected. Similarly, if the value of $flag_{ijkn}$ is 0, the viewpoint will be removed from the set.

After the aforementioned processing, the viewpoints will be evenly distributed around the structure to be inspected, as depicted in Fig.2(c), ensuring the completeness of the viewpoint set's coverage of the structure's surface. The distance between the viewpoints and the structure to be inspected meets both the UAV's safety requirements and the camera's detection requirements, thereby guaranteeing the safety of the UAV's inspection process and the accuracy and validity of the collected data.

3.2 | Viewpoint filtering

When utilizing UAV for 3D structural surface inspection, it is imperative that the camera faces the surface of the structure to accurately capture its surface information, enabling effective observation and analysis of the 3D structural surface. Therefore, this paper proposes a viewpoint filtering method based on surface normal vectors, which calculates the effective inspection area of viewpoints by computing the angle between the optical axis direction of the viewpoint camera and the normal vector of the 3D structural surface to be inspected. The viewpoints are then evaluated based on their effective inspection areas, and those that do not meet the effective inspection requirements are filtered out, thereby ensuring the inspection quality and validity of the drone's surface inspection. Point cloud models, composed of a large number of discrete points, can accurately describe the geometric shape and details of 3D structures. Therefore, the effective inspection area of each viewpoint can be reflected by the number of validly inspected points of the model within its inspection range. The camera, as the most commonly used sensor in the 3D inspection tasks of UAV, can quantitatively express its inspection range through a view frustum. The specific shape of the view frustum is a four-sided frustum composed of a front clipping plane, a back clipping plane, and four other planes, as shown in Fig.3(a). The positional relationship between the view frustum corresponding to the viewpoint in a simplified two-dimensional state and the object to be detected is depicted in Fig.3(b). It can be observed that for each viewpoint's corresponding UAV pose, the surface of the object within its view frustum cannot be fully detected due to occlusions. Therefore, occlusion elimination is necessary to filter out points that cannot be effectively detected due to occlusions. Specifically, the occlusion of a point can be determined by calculating the number of intersections between the line segment formed by the point and the camera's position

and the model. The specific expression is as follows,

$$O(p) = \begin{cases} 0, N_{inter}(p) = 0 \\ 1, N_{inter}(p) \neq 0 \end{cases} \tag{5}$$

where $O(p)$ is the occlusion function value of the point p; $N_{inter}(p)$ is the number of intersection between the line segment formed by the point p and the camera's position and the model. Therefore, the process of occlusion culling can be represented as,

$$P_{occ} = \{p \mid O(p) = 0\} \tag{6}$$

where P_{occ} is potint cloud after removing occlusion culling.

After the occlusion culling, the remaining points are directly detectable by the viewpoint. However, if the angle between the camera optical axis corresponding to the viewpoint and the surface to be detected is excessively large, it will adversely affect the inspection quality, rendering these surfaces ineligible for calculation in the effective inspection area. The method proposed in this paper calculates the angle between the normal vector of each remaining point and the camera optical axis, resulting in a set of effectively detectable point cloud points. Based on this, the effective inspection area of the viewpoint is calculated, and the process of angle calculation is illustrated in Fig.3(c).

The set of neighboring points for the remaining points after occlusion culling can be represented as,

$$P_r(p_{occ}) = \{p_1, p_2, ..., p_n\}, n \in N^* \tag{7}$$

where $P_r(p_{occ})$ is set of points within the neighborhood of point p_{occ} radius r. Assuming the existence of a plane that minimizes the sum of squares of the distances between points in $P_r(p_{occ})$ and that plane, and takes the normal vector of that plane as the normal vector of the point p_{occ}. Use the Eq .8 to represent the fitted plane of points in $P_r(p_{occ})$.

$$z = ax^2 + by^2 + c \tag{8}$$

The parameters of the fitted plane can be obtained by solving the following equation:

$$(a, b, c)^* = \min \sum_{i=1}^{i=n} (z_i - (ax_i + by_i + c))^2 \tag{9}$$

where $(a, b, c)^*$ represents the parameters of the fitted plane; x_i, y_i, z_i are the coordinates of points in $P_r(p_{occ})$. The normal vector of the obtained fitted plane, which is also the normal vector of the point p_{occ}, can be denoted as Eq .10.

$$Vec_p = (a, b, -1) \tag{10}$$

After obtaining the normal vectors of all remaining points within the inspection range of a viewpoint, it is necessary to calculate the angle between them and the optical axis of the camera corresponding to the viewpoint, in order to determine whether the points can be effectively inspected by that viewpoint. The expression of the camera optical axis direction vector in the world coordinate system is as follows:

$$Vec_{cam} = -{}_C^W R^* Z_{cam} \tag{11}$$

where ${}_C^W R$ represents the rotation transformation matrix between the world coordinate system and the camera coordinate system; Z_{cam} is the direction vector of the camera optical axis in the camera coordinate system. Therefore, the angle $\theta(p_{occ})$ between the normal vector of the point p_{occ} and the camera optical axis can be calculated using the Eq. 12.

$$\theta(p_{occ}) = \arccos\left(\frac{Vec_P \cdot Vec_{cam}}{|Vec_P| * |Vec_{cam}|}\right) \tag{12}$$

Afterwards, the calculated angle theta $\theta(p_{occ})$ is compared with a pre-set threshold θ_0 to retain the points that can be effectively inspected, the process can be represented as,

$$P_{filter} = \{p \mid \theta(p) < \theta_0\} \tag{13}$$

where P_{filter} represents the final point cloud set that can be effectively inspected by the viewpoint.

Finally, the inspection effectiveness of the viewpoints is evaluated based on the obtained P_{filter}. Viewpoints that are unable to complete the surface inspection task will be eliminated. Eq. (14) delineates the specific logic of this filtering process,

$$S_{ijkn} = \frac{Num(P_{filter})}{Num(P_{total})}$$
$$flag_{ijkn} = \begin{cases} 1, S_{ijkn} > S_0 \\ 0, S_{ijkn} < S_0 \end{cases} \tag{14}$$

where S_{ijkn} represents the effective inspection evaluation value of a viewpoint; P_{total} denotes the set of model point cloud; S_0 is the threshold for the effective inspection evaluation value. It is an intuitive and effective method to measure the effectiveness of a viewpoint's inspection by calculating the ratio between the effectively inspected point cloud set and the model point cloud set. This approach accurately reflects the inspection performance of a viewpoint.

The viewpoint filtering method based on normal vectors accurately determines whether a point within the inspection range can be effectively detected by a specific viewpoint by calculating the angle between the normal vector of the point and the camera's optical axis. This approach avoids issues such as inaccurate inspection and reduced inspection quality caused by an excessively large angle between the camera's optical axis and the surface of the structure to be inspected, thereby enhancing the accuracy and effectiveness of the drone surface inspection path planning algorithm. Additionally, this method does not rely on specific scenes or structures, making it highly versatile and applicable. Moreover, its principle is simple and intuitive, requiring no complex mathematical models or computational processes, resulting in high operability and reliability in practical applications.

4 | INTEGRATED VIEWPOINT EVALUATION-BASED VIEWPOINT SELECTION

After obtaining a complete, safe, and effective set of viewpoints, selecting the viewpoints to generate the UAV inspection path is a crucial factor determining the inspection capability and efficiency during the UAV inspection process. In the task of path planning for surface inspection of large-scale 3D structures, the increase in the number of viewpoints leads to an expanded search space, while factors such as coverage and path length also need to be considered, posing significant challenges to the viewpoint selection strategy. Therefore, this paper proposes a viewpoint selection method based on integrated viewpoint evaluation, which combines the integrated viewpoint evaluation value containing global, local information, and past search experience with MCTS. This approach avoids getting stuck in local optima during the viewpoint selection process, reduces surface inspection path redundancy, and improves the efficiency of UAV inspection tasks.

4.1 | Child viewpoint sequence generation

The core idea of the proposed surface inspection UAV path planning method in this paper is to iteratively select the optimal child viewpoint from the child viewpoint sequence of the current viewpoint, thereby gradually expanding the path. To achieve this, a child viewpoint sequence needs to be generated for each viewpoint. Specifically, for a given viewpoint VP_i, if there exists another viewpoint VP_j such that the distance between them is less than a predefined child viewpoint distance threshold d_{th}, then viewpoint VP_j will become a member of the child viewpoint sequence of viewpoint VP_i. This process can be formally expressed as,

$$\text{dis}(VP_i, VP_j) \leq d_{\text{th}} \Rightarrow VP_j \in child(VP_i) \tag{15}$$

where $\text{dis}(VP_i, VP_j)$ is the distance between two viewpoints; $child(VP_i)$ is a child viewpoint sequence of VP_i. Therefore, all other viewpoints within a certain range of viewpoints VP_i will be added to its child viewpoint sequence.

This distance-based child viewpoint sequence generation method ensures that the child viewpoints originate from regions near the current viewpoint, thereby guaranteeing that the generated drone UAV paths can better capture the correlation of local information while also maintaining spatial continuity. Moreover, the distance threshold d_{th} can be adjusted according to specific task requirements, enabling the method to obtain a more suitable child viewpoint sequence and demonstrating its adaptability in various scenarios.

Algorithm 2 Integrated viewpoint evaluation-based viewpoint selection algorithm

---

Input: 1)Viewpoint set generated by Algorithm 1, 2)distance threshold d_{th},
　　3)exploration constant c_1, 4) coefficient of child viewpoint coverage c_2.
Output: UAV 3D structure surface inspection path: *Path*.

1: Generate child viewpoint sequence by d_{th} and viewpoint set thorough distance-based method (Eq.(15))
2: Create root viewpoint VP_{cur}
3: **while** Coverage of *Path* lower than the requirement **do**
4: 　**if** $\exists\ iS(VP_{chi}) = 0, VP_{chi} \in child(VP_{cur})$ **then**
5: 　　$VP_{exp} \leftarrow$ EXPANSION(VP_{cur})
6: 　　$R, simPath \leftarrow$ SIMULATION($VP_{exp}, Path$)
7: 　　BACKPROPAGATION($R, simPath$)
8: 　**else**
9: 　　$VP_{cur} \leftarrow$ SELECTION(VP_{cur})
10: 　　Add VP_{cur} to *Path*
11: 　**end if**
12: **end while**
13: **return** Outputs
14: **function** EXPANSION(VP_{cur})
15: 　$VP_{exp} \leftarrow \underset{VP_{chi}}{\arg\min}\, iS(VP_{chi})$ (Eq.(16))
16: 　**return** VP_{exp}
17: **end function**
18: **function** SELECTION(VP_{cur}, c_1, c_2)
19: 　**return** $\underset{VP_{chi}}{\arg\max} \frac{Q(VP_{chi})}{N(VP_{chi})} + c_1 \sqrt{\frac{\ln N(VP_{cur})}{N(VP_{chi})}} + c_2 \frac{C_{chi}}{C_{std}}$
20: **end function**
21: **function** SIMULATION($VP_{exp}, Path$)
22: 　$VP_{sim} \leftarrow VP_{exp}$
23: 　$simPath \leftarrow Path$
24: 　**while** Coverage of *simPath* lower than the requirement **do**
25: 　　$VP_{sim} \leftarrow \underset{VP_s \in child(VP_{sim})}{\arg\max} CIns(VP_s)$(Eq.17)
26: 　　Add VP_{sim} to *simPath*
27: 　**end while**
28: 　**return** $\frac{C_{final} - C_{start}}{n_{sim} * C_{std}}$, *simPath*
29: **end function**
30: **procedure** BACKPROPAGATION($R, simPath$)
31: 　**for** Each $VP_i \in simPath \&\& VP_i \notin Path$ **do**
32: 　　$N(VP_i) \leftarrow N(VP_i) + 1$
33: 　　$Q(VP_i) \leftarrow Q(VP_i) + R$
34: 　**end for**
35: **end procedure**

4.2 | Viewpoint selection

Traditional sampling-based methods for UAV surface inspection path planning often consider only the relevant information of child viewpoints during the path expansion, such as selecting the child viewpoint with the greatest coverage increase as the next viewpoint. However, this viewpoint selection strategy can easily lead to the path search process falling into local optima, resulting in redundant paths and reduced UAV inspection efficiency. Therefore, the viewpoint selection method proposed in this paper utilizes MCTS combined with a integrated viewpoint evaluation method, which integrates global and local search information with search experience to select child viewpoints. By repeatedly iterating through the four stages of expansion,

simulation, backpropagation, and selection, it can more comprehensively explore the search space, better utilize prior global model information, avoid redundant inspection paths, and enhance the inspection efficiency and energy utilization efficiency of UAV.

4.2.1 | Expansion

Assuming $child(VP_{cur})$ is a child viewpoint sequence of the current viewpoint VP_{cur}, the expansion process involves selecting child viewpoint from $child(VP_{cur})$ that have not yet been expanded to prepare for the next simulation process. This expansion process can be represented as,

$$VP_{\exp} = \arg\min_{VP_{chi}} \mathrm{iS}(VP_{chi}), VP_{chi} \in child(VP_{cur})$$

$$\mathrm{iS}(VP_{chi}) = \begin{cases} 1, VP_{chi} \text{ was expanded} \\ 0, VP_{chi} \text{ wasn't expanded} \end{cases} \tag{16}$$

where $VP_{\exp}$ is expanded child viewpoint; $\mathrm{iS}(VP_{chi})$ is expanding status of VP_{chi}.

4.2.2 | Simulation

The simulation process serves as a crucial step in evaluating the quality of current child viewpoints. The approach proposed in this paper utilizes guided simulation, which introduces viewpoint coverage growth information in a targeted manner to enhance the coverage and efficiency of path planning. The simulation process commences from the expanded child viewpoint $VP_{\exp}$, continuously selecting viewpoints to form a simulated path until the desired criteria are met. This process can be expressed as,

$$VP_{\sim} = \arg\max_{VP_s} \mathrm{CIns}(VP_s), VP_s \in child(VP_{\sim}) \tag{17}$$

where VP_{sim} represents simulation viewpoint, and the first simulated viewpoint is expanded child viewpoint $VP_{\exp}$ obtained from the expansion process; $\mathrm{CIns}(VP_s)$ stands for the increase in coverage of the simulated path after adding the viewpoint P_s to it. This step is repeated continuously during the simulation until the increase in coverage of the simulated path reaches a pre-set standard. This guided simulation method based on coverage selects child viewpoints with the greatest potential for coverage increase, enabling the simulation process to preferentially search for directions that can enhance the overall coverage of the path. This approach aims to expedite convergence towards potential areas of complete coverage, accelerate the simulation search process, and improve the efficiency of path planning. Moreover, it takes into account the increase in coverage after adding each child viewpoint to the simulated path. This approach allows for a more thorough utilization of local information, resulting in more comprehensive and accurate path planning, ultimately improving the execution of UAV surface inspection tasks.

4.2.3 | Backpropagation

To backpropagate the simulation path evaluation results obtained from the coverage based guided simulation process to each viewpoint involved, accurately reflecting the quality and potential value of each viewpoint, and guiding the selection process to better select child viewpoints, it is necessary to perform a simulation result backpropagating process. During the backpropagation process, two characteristic values need to be updated for each viewpoint: $N(VP)$, representing the number of visits to the viewpoint, and $Q(VP)$, indicating the empirical average result of the viewpoint. When backpropagating, each viewpoint feature value involved in the simulation process needs to be updated according to the following equation,

$$\begin{cases} N(VP) = N(VP) + 1 \\ Q(VP) = Q(VP) + R \end{cases} \tag{18}$$

where R represents the outcome of the simulation. Specifically, during the ackpropagation process, the number of visits to each simulated viewpoint is incremented by 1, while the empirical average result value of the viewpoint is updated based on the simulation result R. In traditional MCTS algorithms, simulation outcomes are often expressed as binary results, representing success or failure with simulation result values R of 0 or 1. However, this approach lacks an evaluation of the extent of path

coverage, failing to provide a nuanced measure of the quality of simulated paths. This can lead to a lack of understanding of the comprehensiveness of the search process and the changes in coverage at different stages, preventing the reflection of real-time coverage variations. Therefore, in the proposed viewpoint selection method, the standard coverage is utilized to calculate the R value for each simulation, resulting in a more flexible and accurate measurement of simulation outcomes. This approach enables the accurate reflection of coverage variations through the simulation process at different stages of path planning, ultimately facilitating the selection of optimal viewpoints to form a complete coverage inspection path. Specifically, the calculation of R in the proposed method is conducted as follows,

$$R = \frac{C_{final} - C_{start}}{n_{sim} * C_{std}} \qquad (19)$$

where C_{final} represent the coverage of the simulated path after adding the final simulated viewpoint; C_{start} represent the coverage of the path before the simulation starts,;n_{sim} represent the number of viewpoints added to the simulated path during the simulation; C_{std} represent the standard coverage. The specific calculation of the standard coverage is as follows,

$$C_{std} = \frac{C_{total}}{n_{total}} \qquad (20)$$

where C_{total} represents the total coverage of the effective detection viewpoint set generated after filtering based on position and normal vectors; n_{total} represents the number of viewpoints in the viewpoint set. The standard coverage calculated in this manner represents the expected increase in path coverage for each additional viewpoint, comprehensively reflecting the coverage capability of the viewpoint set.

The backpropagation method based on the standard coverage incorporates the increase in overall simulation path coverage, providing an intuitive and specific reflection of the quality of the simulation path. Additionally, by combining the number of viewpoints added to the simulation path with the standard coverage, it considers the comprehensive impact of simulation effectiveness and the selected number of viewpoints, enabling a comprehensive evaluation of the simulation results. Standardizing the simulation result value by dividing it by the product of the number of viewpoints added to the simulasimulationted path and the standard coverage facilitates the quantification of the contribution of the simulation path to the overall coverage. This backpropagation approach is suitable for various scales of UAV surface inspection path planning problems.

4.2.4 | Selection

After expanding and simulating all child viewpoints within the current viewpoint VP_{cur}, the visit counts and empirical average result value of each child viewpoint have been updated. Consequently, a selection of the child viewpoints needs to be made based on these two metrics. The traditionally MCTS algorithm utilizes the Upper Confidence Bound Apply to Trees (UCT) value to compute the selection probability for each child node. The formula for this computation is as follows,

$$\text{UCT}(VP_{chi}) = \frac{Q(VP_{chi})}{N(VP_{chi})} + c^* \sqrt{\frac{\ln N(VP_{cur})}{N(VP_{chi})}}, \qquad (21)$$
$$VP_{chi} \in child(VP_{cur})$$

where VP_{cur} represents the current viewpoint, and c represents the exploration constant. Then, the child viewpoint with the highest UCT value is selected as the next viewpoint for expanding the path, as Eq. 22.

$$VP_{cur} = \arg\max_{VP_{chi}} \text{UCT}(VP_{chi}), VP_{chi} \in child(VP_{cur}) \qquad (22)$$

A child viewpoint with a higher empirical average result value Q indicates a superior performance during previous simulations. Meanwhile, the confidence bound term $\sqrt{\frac{\ln N(VP_{cur})}{N(VP_{chi})}}$ enables child viewpoint with fewer visits to have a higher UCT value. This balance enables the algorithm to not only favor the selection of known better viewpoints but also explore potentially better unknown viewpoints. The exploration constant c can be flexibly adjusted to accommodate viewpoint selection tasks of different scales.

However, in practical applications of UAV surface inspection path planning, the selection of child viewpoints not only needs to consider the global reward and exploration status but also the coverage status within the local range to comprehensively evaluate the quality of child viewpoints. During the path expansion process, due to overlapping coverage surfaces, the addition of viewpoints may reduce the growth of coverage for other unselected viewpoints. This dynamic change can affect the accuracy

and reliability of the UCT value. Therefore, in the method proposed in this paper, local information is integrated into the child viewpoint selection process, and an Integrated Viewpoint Evaluation (IVE) based on the UCT value is proposed,

$$\text{IVE}(VP_{chi}) = \frac{Q(VP_{chi})}{N(VP_{chi})} + c_1 \sqrt{\frac{\ln N(VP_{cur})}{N(VP_{chi})}} + c_2 \frac{C_{chi}}{C_{std}} \qquad (23)$$

where C_{chi} represent the growth of coverage for child viewpoint; c_1 denote the exploration constant; c_2 represent the coefficient of child viewpoint coverage. Therefore, the process of viewpoint selection can be expressed as Eq. 24.

$$VP_{cur} = \arg\max_{VP_{chi}} \text{IVE}(VP_{chi}), VP_{chi} \in child(VP_{cur}) \qquad (24)$$

This method of viewpoint evaluation takes into account both the average performance of child viewpoints during previous search processes and the relative coverage growth within a local range. It can also handle dynamic changes in viewpoint coverage during path search, providing a more comprehensive evaluation of the quality of child viewpoints. The viewpoint selection method based on the integrated viewpoint evaluation value introduces the coverage growth of child viewpoints and standardizes it using the standard coverage.

This approach facilitates balancing global and local factors during path expansion, avoids path redundancy caused by overlapping viewpoint coverage, and effectively copes with dynamic changes resulting from overlapping viewpoint coverage. Additionally, the UCT value, as a crucial component of the integrated viewpoint evaluation value, retains the experience of simulation and exploration processes while balancing exploration and exploitation, rendering the algorithm more robust and adaptive during path expansion. Therefore, employing the integrated viewpoint evaluation value for viewpoint selection contributes to a more comprehensive and accurate assessment of child viewpoints in the path expansion for drone surface inspection, ultimately enhancing the inspection quality and efficiency of the path.

5 | EXPERIMENTAL RESULTS AND DISCUSSION

5.1 | Simulation experiments

To validate the effectiveness and feasibility of the proposed IPP algorithm for UAV surface inspection, a simulation study was conducted on a typical 3D structure, with a comparative analysis against three other commonly used path planning algorithms for UAV surface inspection. The simulation experiments were performed using ROS-Melodic on an Ubuntu 18.04 system, with a workstation equipped with an Intel Core i5-10400F 2.9 GHz processor and 16GB of RAM. To accurately and quantitatively assess the performance of different UAV surface IPP algorithms, metrics such as the total path length, the number of viewpoints along the path, the inspection time, and the defective coverage ratio were proposed. During the inspection process, the UAV needs to hover at each viewpoint to capture surface information, thus the inspection time is influenced by both the path length and the number of viewpoints. The defective coverage ratio refers to the proportion of the surface area with excessive angles between the normal vectors and the camera optical axis, relative to the total surface area to be inspected.

The complex shapes of the hoaHakanai'a statue pose unique challenges for UAV 3D surface IPP algorithms, thus they are often widely used to test the algorithm's ability to handle unstructured objects with complex shapes, as well as its completeness and accuracy of coverage. Therefore, this study first selected the hoaHakanai'a statue as the research subject. By applying the proposed UAV surface inspection path planning algorithm based on normal vector viewpoint filtering and comprehensive viewpoint evaluation, a comprehensive comparison was made with the ASSCPP, Structural Inspection Planner, and TSP with LKH algorithm to test the performance of the proposed algorithm. The specific results are presented in Table 1 and Fig. 4. In the figure, the positions of the arrows represent the UAV locations corresponding to the viewpoints, while the directions of the arrows indicate the direction of the camera optical axis corresponding to each viewpoint.

In the compared methods, Structural Inspection Planner and TSP with LKH generate viewpoints by sampling each surface of the standard triangular mesh. Therefore, their path length and the number of viewpoints are greatly influenced by the model's precision. When the model's precision is high, there are more surfaces, leading to an increase in the number of viewpoints, which results in redundant paths, increased inspection time, and reduced inspection efficiency. Conversely, when the model's precision is low, a single viewpoint may fail to fully cover its corresponding surface, degrading the inspection quality. Consequently, in the path planning experiments conducted on the hoaHakanai'a statue, the proposed method in this paper achieved a reduction in
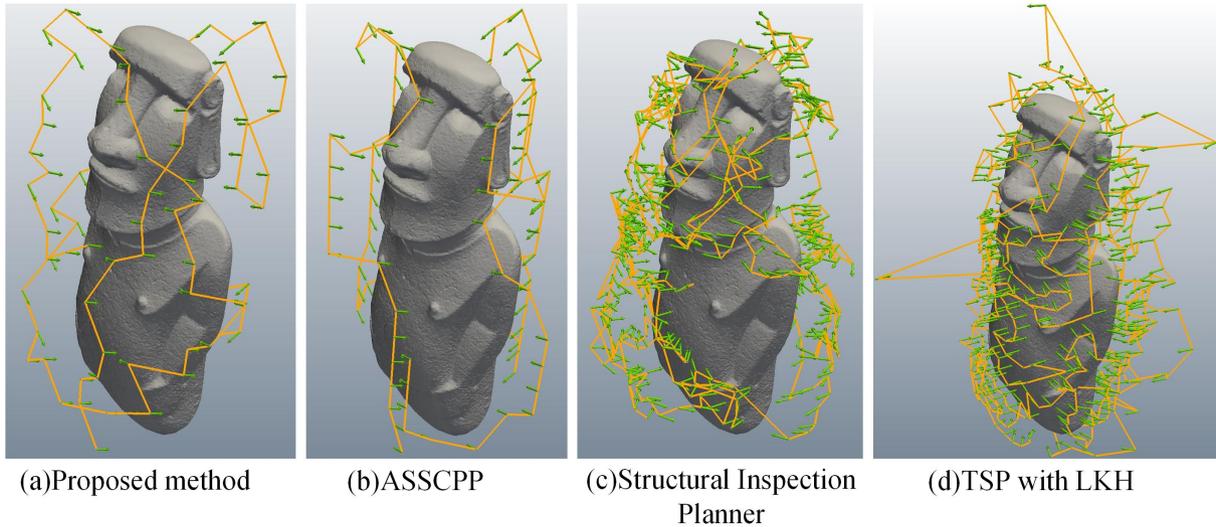
| (a)Proposed method | (b)ASSCPP | (c)Structural Inspection Planner | (d)TSP with LKH |

FIGURE 4 Simulation experiment results of surface inspection path planning for hoaHakanai'a statue.

TABLE 1 Simulation experiment data results of surface inspection path planning for hoaHakanai'a statue

Metrics	Algorithm			
	Proposed method	ASSCPP	Structural Inspection Planner	TSP with LKH
Path Length (/m)	159.14	163.31	493.18	577.85
Viewpoints Number	84	94	556	556
Inspection Time (/s)	327.14	351.31	1605.18	1689.85
Defective Coverage Ratio (%)	4.93	9.98	9.84	11.16

path length by 67.7% and 72.5%, respectively, compared to Structure Planner and TSP with LKH algorithms. Additionally, the inspection time was reduced by 79.6% and 80.6%, respectively, while the defective coverage ratio also decreased by 40.9% and 55.8%, respectively.

On the other hand, the ASSCPP algorithm, which employs an adaptive sampling strategy for viewpoint generation, demands less precision in models. However, its viewpoint generation process is primarily driven by coverage metrics, overlooking inspection quality. Consequently, in the hoaHakanai'a statue path planning experiment, the proposed algorithm in this paper exhibits a 50.6% reduction in defective coverage ratio compared to the ASSCPP algorithm. Furthermore, our approach leverages a MCTS algorithm based on integrated viewpoint evaluation, enabling the optimal utilization of both global and local information. As a result, our algorithm achieves a 2.5% decrease in path length and a 6.9% reduction in inspection time compared to the ASSCPP algorithm in the hoaHakanai'a statue path planning experiment.

Bridges, as crucial transportation hubs, require comprehensive inspections and maintenance in practical applications. These structures, often comprising of multi-level components such as bridge decks, piers, and supporting structures, exhibit significant vertical and horizontal variations. This complexity poses significant challenges in achieving comprehensive path planning for UAVs conducting bridge surface inspections. Therefore, this study selects bridge unit as the research object to examine whether the proposed algorithm can meet the demands for detection quality and efficiency in UAV surface inspections of multi-level structures. Furthermore, a comparative analysis with other existing path planning algorithms for UAV surface inspections is conducted to demonstrate the characteristics of the proposed algorithm in this context. The specific results are presented in Table 2 and Fig. 5.

Similar to the path planning experiment for the hoaHakanai'a statue, in the simulation experiment for bridge unit surface inspection path planning, the method proposed in this paper achieved a significant reduction in path length compared to the Structural Inspection Planner and TSP with LKH, with decreases of 77.64% and 78.7% respectively. The inspection time also saw an order-of-magnitude improvement, while the defective coverage ratio were reduced by 31.7% and 62.9% respectively.
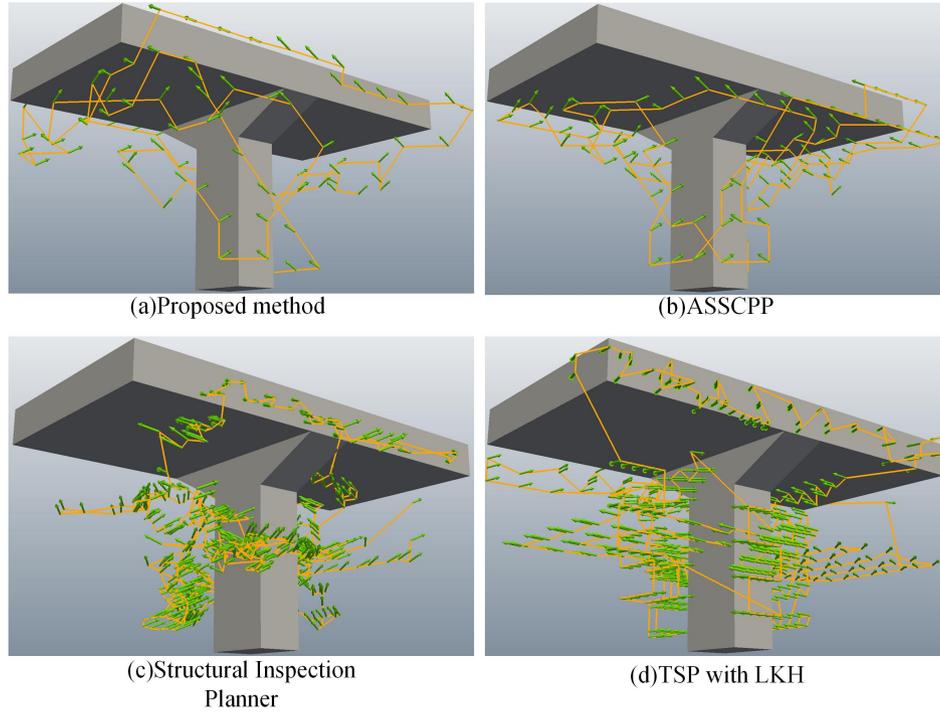
(a)Proposed method (b)ASSCPP

(c)Structural Inspection Planner (d)TSP with LKH

F I G U R E 5 Simulation experiment results of surface inspection path planning for bridge unit.

When compared to the ASSCPP, the proposed algorithm in this paper reduced the path length by 58.76%. Additionally, it reduced the inspection time by 38.57% and the defective coverage ratio by 39.6%.

T A B L E 2 Simulation experiment data results of surface inspection path planning for bridge unit

Metrics	Algorithm			
	Proposed method	ASSCPP	Structural Inspection Planner	TSP with LKH
Path Length (/m)	154.31	187.07	344.95	362.56
Viewpoints Number	84	106	538	538
Inspection Time (/s)	322.31	399.07	1420.95	1438.56
Defective Coverage Ratio (%)	5.74	9.51	8.42	15.48

Based on the experimental results and comparative analysis of the surface inspection path planning experiments conducted on the hoaHakanai'a statue and bridge unit, it is evident that the proposed UAV surface inspection path planning algorithm utilizing normal vector viewpoint filtering and integrated viewpoint evaluation outperforms the commonly used ASSCPP, Structural Inspection Planner, and TSP with LKH in terms of both efficiency and effectiveness in planning surface inspection paths for 3D structures. This algorithm requires lower model precision during the planning process, can integrate global and local information to avoid redundant paths, and simultaneously reduces the defective coverage ratio, ensuring the inspection quality of the generated paths.

5.2 | Real world experiment

To test the effectiveness of the proposed UAV surface inspection path planning algorithm in real-world scenarios, this study conducted a real world path planning experiment. The Dij Mini 4 pro, which was used in this experiment, possesses omnidirectional

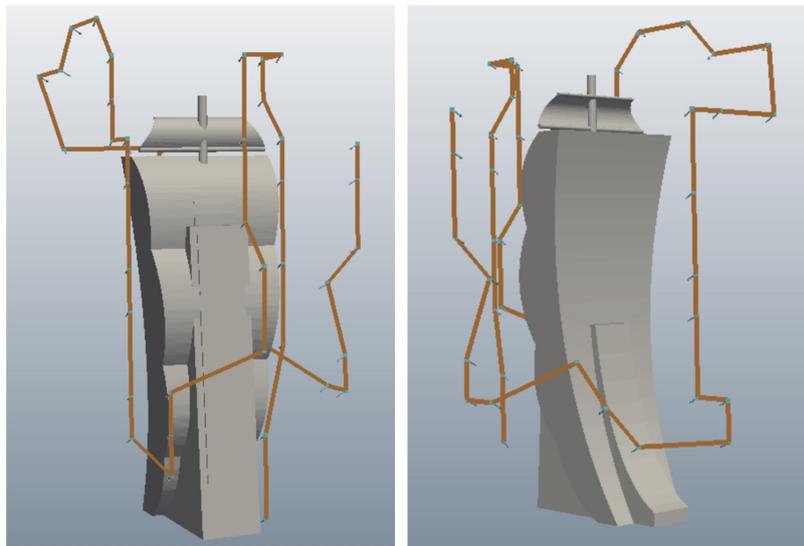**F I G U R E 6** Sail sculpture used in real world experiment.

F I G U R E 7 The sail sculpture model and its corresponding inspection path.

obstacle avoidance capabilities and can perform waypoint flights based on pre-set waypoint files, with an effective detection range of 1-6 meters.

The research object for this real world experiment was the sail sculpture located in the Western China Science And Technology Innovation Harbour. This sculpture, which is depicted in Fig. 6, has no surrounding obstacles, a height exceeding 15 meters, and belongs to a large-scale 3D structure. Additionally, its unique shape and complex structure provide an ideal testing platform for the evaluation of UAV path planning algorithms for 3D surface inspection.

Before conducting real world experiments using UAV, a rough model of the sail was created to obtain the surface inspection path, as shown in Fig. 7.

To transform the inspection path into UAV waypoint information, the data collection for surface inspection of the sail sculpture was achieved by importing the information into the UAV. The flight posture and perspective of the UAV during the physical experiment can be observed clearly through the video link: www.bilibili.com/BV13z421Y7L1. During the inspection path operation, the UAV ran for a total of 113 seconds, with a total path length of 42m. From the video, it is evident that the UAV flew with stability, capturing intricate surface textures and details of the sail sculpture with no significant blurring or defocusing, indicating a high level of clarity and accuracy in the surface information collected by the UAV.

Utilizing the COLMAP software, the surface information gathered by the UAV during the physical experiment was reconstructed into a three-dimensional model. As depicted in Fig. 8, the resulting reconstruction is clear and devoid of noticeable defects, suggesting that the chosen path effectively achieved comprehensive coverage of the sail sculpture's surface. This, in turn, validates the completeness of the surface inspection data collection. The results of the real world experiments demonstrate that the proposed UAV path planning algorithm for 3D structural surface inspection can accurately and efficiently accomplish

FIGURE 8 Reconstruction results of sail sculpture.

the task of collecting surface inspection data. The generated surface inspection path is capable of comprehensively covering the surface of the 3D structure.

6 | CONCLUSION

In addressing the challenges of model dependency and unpredictable inspection quality in path planning algorithms for unmanned aerial vehicles performing 3D structural surface inspection tasks, this paper proposes a viewpoint generation method based on normal vector filtering. By uniformly sampling the sampling space, an initial set of viewpoints is generated that is independent of the shape of the object to be inspected and evenly distributed. The initial set of viewpoints is then filtered based on normal vectors, eliminating those that cannot effectively detect the surface, thus ensuring the completeness and effectiveness of the UAV surface inspection task.

Regarding the viewpoint selection process, this paper introduces a integrated viewpoint evaluation method to address the issues of path redundancy and difficulty in utilizing global information in commonly used surface inspection path planning algorithms. The integrated evaluation method incorporates factors such as global and local information as well as search experience into the viewpoint selection process. Additionally, Monte Carlo Tree Search is employed to reduce path redundancy, thereby improving the efficiency and quality of the UAV surface inspection path planning.

However, the proposed method still has some limitations. Some viewpoints generated by uniform sampling may have excessive overlap in the detection range, potentially leading to excessive coverage of certain areas of the surface to be inspected while other areas receive insufficient coverage, resulting in uneven inspection quality. Therefore, future work will focus on further optimizing the sampling strategy by introducing a dynamic sampling density adjustment mechanism.

AUTHOR CONTRIBUTIONS
Yunlong Wang: Conceptualization, Data curation, Investigation, Methodology, Project administration, Software, Supervision,Validation,Visualization, Writing-original draft, Writing-review & editing . Shaoke Wan: Funding acquisition, Validation, Writing-review & editing. Rongcan Qiu: Writing-original draft, Writing-review & editing. Xiaohu Li: Funding acquisition, Validation, Writing-review & editing.

FINANCIAL DISCLOSURE
There are no financial conflicts of interest to disclose

CONFLICT OF INTEREST

The authors declare that they have no known competing financial interests or personal relationships that could have appeared to influence the work reported in this paper.

DATA AVAILABLE STATEMENT

The data that support the findings of this study are available onrequest from the corresponding author. The data are not publiclyavailable due to privacy or ethical restrictions.

REFERENCES

1. Feng L, Katupitiya J. UAV-based persistent full area coverage with dynamic priorities. *Robotics and Autonomous Systems*. 2022;157:104244. doi: https://doi.org/10.1016/j.robot.2022.104244
2. Kanistras K, Martins G, Rutherford MJ, Valavanis KP. A survey of unmanned aerial vehicles (UAVs) for traffic monitoring. *2013 International Conference on Unmanned Aircraft Systems, ICUAS 2013 - Conference Proceedings*. 2013:221 – 234. doi: 10.1109/ICUAS.2013.6564694
3. Pham HX, La HM, Feil-Seifer D, Deans M. A distributed control framework for a team of unmanned aerial vehicles for dynamic wildfire tracking. *IEEE International Conference on Intelligent Robots and Systems*. 2017;2017-September:6648 – 6653. Cited by: 88; All Open Access, Green Open Accessdoi: 10.1109/IROS.2017.8206579
4. Lottes P, Khanna R, Pfeifer J, Siegwart R, Stachniss C. UAV-based crop and weed classification for smart farming. *Proceedings - IEEE International Conference on Robotics and Automation*. 2017:3024 – 3031. Cited by: 297doi: 10.1109/ICRA.2017.7989347
5. Barrientos A, Colorado J, Cerro JD, et al. Aerial remote sensing in agriculture: A practical approach to area coverage and path planning for fleets of mini aerial robots. *Journal of Field Robotics*. 2011;28(5):667 – 689. Cited by: 230; All Open Access, Green Open Accessdoi: 10.1002/rob.20403
6. Dorling K, Heinrichs J, Messier GG, Magierowski S. Vehicle Routing Problems for Drone Delivery. *IEEE Transactions on Systems, Man, and Cybernetics: Systems*. 2017;47(1):70-85. doi: 10.1109/TSMC.2016.2582745
7. Altshuler Y, Yanovsky V, Wagner IA, Bruckstein AM. Efficient cooperative search of smart targets using UAV Swarms. *Robotica*. 2008;26(4):551 – 557. Cited by: 75doi: 10.1017/S0263574708004141
8. Renzaglia A, Reymann C, Lacroix S. Monitoring the evolution of clouds with UAVs. *Proceedings - IEEE International Conference on Robotics and Automation*. 2016;2016-June:278 – 283. Cited by: 23; All Open Access, Green Open Accessdoi: 10.1109/ICRA.2016.7487145
9. Khan A, Gupta S, Gupta SK. Emerging UAV technology for disaster detection, mitigation, response, and preparedness. *Journal of Field Robotics*. 2022;39(6):905-955. doi: https://doi.org/10.1002/rob.22075
10. Zhao N, Lu W, Sheng M, et al. UAV-assisted emergency networks in disasters. *IEEE Wireless Communications*. 2019;26(1):45 – 51. Cited by: 479; All Open Access, Green Open Accessdoi: 10.1109/MWC.2018.1800160
11. Mozaffari M, Saad W, Bennis M, Debbah M. Efficient Deployment of Multiple Unmanned Aerial Vehicles for Optimal Wireless Coverage. *IEEE Communications Letters*. 2016;20(8):1647 – 1650. Cited by: 843; All Open Access, Bronze Open Access, Green Open Accessdoi: 10.1109/LCOMM.2016.2578312
12. Ivic S, Crnkovic B, Grbcic L, Matlekovic L. Multi-UAV trajectory planning for 3D visual inspection of complex structures. *Automation in Construction*. 2023;147. doi: 10.1016/j.autcon.2022.104709
13. Almadhoun R, Taha T, Seneviratne L, Dias J, Cai G. A survey on inspecting structures using robotic systems. *International Journal of Advanced Robotic Systems*. 2016;13(6):1729881416663664. doi: 10.1177/1729881416663664
14. Wang JH, Ueda T. A review study on unmanned aerial vehicle and mobile robot technologies on damage inspection of reinforced concrete structures. *Structural Concrete*. 2023. doi: 10.1002/suco.202200846
15. Shang Z, Bradley J, Shen Z. A co-optimal coverage path planning method for aerial scanning of complex structures. *Expert Systems with Applications*. 2020;158:113535. doi: https://doi.org/10.1016/j.eswa.2020.113535
16. Munishkin AA, Milutinović D, Casbeer DW. Min–max time efficient inspection of ground vehicles by a UAV team. *Robotics and Autonomous Systems*. 2020;125:103370. doi: https://doi.org/10.1016/j.robot.2019.103370
17. Qu H. Research on UAV Path Planning Algorithm for Bridge Detection. *Harbin Engineering University*. 2018.
18. Wang F, Zou Y, Chen X, et al. Rapid in-flight image quality check for UAV-enabled bridge inspection. *ISPRS Journal of Photogrammetry and Remote Sensing*. 2024;212:230-250. doi: https://doi.org/10.1016/j.isprsjprs.2024.05.008
19. Zhang S, Liu C, Haala N. Guided by model quality: UAV path planning for complete and precise 3D reconstruction of complex buildings. *International Journal of Applied Earth Observation and Geoinformation*. 2024;127:103667. doi: https://doi.org/10.1016/j.jag.2024.103667
20. Shu M, Li Q, Ghafoor A, Zhu J, Li B, Ma Y. Using the plant height and canopy coverage to estimation maize aboveground biomass with UAV digital images. *European Journal of Agronomy*. 2023;151:126957. doi: https://doi.org/10.1016/j.eja.2023.126957
21. SONUGÜR G. A Review of quadrotor UAV: Control and SLAM methodologies ranging from conventional to innovative approaches. *Robotics and Autonomous Systems*. 2023;161:104342. doi: https://doi.org/10.1016/j.robot.2022.104342
22. Halder S, Afsari K. Robots in Inspection and Monitoring of Buildings and Infrastructure: A Systematic Review. *Applied Sciences*. 2023;13(4):2304.
23. Tan Y, Li S, Liu H, Chen P, Zhou Z. Automatic inspection data collection of building surface based on BIM and UAV. *Automation in Construction*. 2021;131:103881. doi: https://doi.org/10.1016/j.autcon.2021.103881
24. Jing W, Deng D, Wu Y, Shimada K. Multi-UAV Coverage Path Planning for the Inspection of Large and Complex Structures. *2020 IEEE/RSJ International Conference on Intelligent Robots and Systems (IROS)*. 2020:1480-1486. doi: 10.1109/iros45743.2020.9341089
25. Dogru S, Marques L. ECO-CPP: Energy constrained online coverage path planning. *Robotics and Autonomous Systems*. 2022;157:104242. doi: https://doi.org/10.1016/j.robot.2022.104242
26. Bohari SN, Amran AU, Zaki NAM, Suhaimi MS, Rasam ARA. Accuracy Assessment of Detecting Cracks on Concrete Wall at Different Distances using Unmanned Autonomous Vehicle (UAV) Images. *IOP Conference Series: Earth and Environmental Science*. 2021;620(1):012005. doi: 10.1088/1755-1315/620/1/012005
27. Iacono M, Sgorbissa A. Path following and obstacle avoidance for an autonomous UAV using a depth camera. *Robotics and Autonomous Systems*. 2018;106:38-46. doi: https://doi.org/10.1016/j.robot.2018.04.005

28. Semiz F, Polat F. Solving the area coverage problem with UAVs: A vehicle routing with time windows variation. *Robotics and Autonomous Systems.* 2020;126:103435. doi: https://doi.org/10.1016/j.robot.2020.103435

29. Hameed I, la Cour-Harbo A, Osen O. Side-to-side 3D coverage path planning approach for agricultural robots to minimize skip/overlap areas between swaths. *Robotics and Autonomous Systems.* 2016;76:36-45. doi: https://doi.org/10.1016/j.robot.2015.11.009

30. Zhang R, Hao G, Zhang K, Li Z. Reactive UAV-based automatic tunnel surface defect inspection with a field test. *Automation in Construction.* 2024;163:105424. doi: https://doi.org/10.1016/j.autcon.2024.105424

31. Li J, Yang X, Yang Y, Liu X. Cooperative mapping task assignment of heterogeneous multi-UAV using an improved genetic algorithm. *Knowledge-Based Systems.* 2024;296:111830. doi: https://doi.org/10.1016/j.knosys.2024.111830

32. Li Y. UAV MOTION PLANNING FOR ROAD BRIDGE INSPECTION TASK. *Harbin Institute of Technology.* 2020. doi: 10.27061/d.cnki.ghgdu.2020.002912

33. Choset H. Coverage of known spaces: The boustrophedon cellular decomposition. *Autonomous Robots.* 2000;9(3):247-253. doi: 10.1023/a:1008958800904

34. Acar EU, Choset H, Rizzi AA, Atkar PN, Hull D. Morse decompositions for coverage tasks. *International Journal of Robotics Research.* 2002;21(4):331-344. doi: 10.1177/027836402320556359

35. Yao P, Cai YG, Zhu Q. Time-optimal trajectory generation for aerial coverage of urban building. *Aerospace Science and Technology.* 2019;84:387-398. doi: 10.1016/j.ast.2018.10.011

36. Kumar K, Kumar N. Region coverage-aware path planning for unmanned aerial vehicles: A systematic review. *Physical Communication.* 2023;59:102073. doi: https://doi.org/10.1016/j.phycom.2023.102073

37. Alexis K, Papachristos C, Siegwart R, Tzes A. Uniform coverage structural inspection path–planning for micro aerial vehicles. *2015 IEEE International Symposium on Intelligent Control (ISIC).* 2015:59-64. doi: 10.1109/ISIC.2015.7307280

38. Zhang C, Qin H, Sun S, et al. JPMDP: Joint base placement and multi-configuration path planning for 3D surface disinfection with a UV-C robotic system. *Robotics and Autonomous Systems.* 2024;174:104644. doi: https://doi.org/10.1016/j.robot.2024.104644

39. Englot B, Hover F. Sampling-Based Coverage Path Planning for Inspection of Complex Structures. *Proceedings of the International Conference on Automated Planning and Scheduling.* 2012;22:29-37. doi: 10.1609/icaps.v22i1.13529

40. Englot B, Hover F. *Planning Complex Inspection Tasks Using Redundant Roadmaps*:327-343; Cham: Springer International Publishing . 2017

41. Bircher A, Kamel M, Alexis K, et al. Three-dimensional coverage path planning via viewpoint resampling and tour optimization for aerial robots. *Autonomous Robots.* 2015;40(6):1059-1078. doi: 10.1007/s10514-015-9517-1

42. Bolourian N, Hammad A. LiDAR-equipped UAV path planning considering potential locations of defects for bridge inspection. *Automation in Construction.* 2020;117. doi: 10.1016/j.autcon.2020.103250

43. Almadhoun R, Taha T, Seneviratne L, Dias J, Cai G. GPU accelerated coverage path planning optimized for accuracy in robotic inspection applications. *2016 IEEE 59th International Midwest Symposium on Circuits and Systems (MWSCAS).* 2016:1-4. doi: 10.1109/MWSCAS.2016.7869968

44. Almadhoun R, Taha T, Gan D, Dias J, Zweiri Y, Seneviratne L. Coverage Path Planning with Adaptive Viewpoint Sampling to Construct 3D Models of Complex Structures for the Purpose of Inspection. *2018 IEEE/RSJ International Conference on Intelligent Robots and Systems (IROS).* 2018:7047-7054. doi: 10.1109/IROS.2018.8593719

45. Silberberg P, Leishman RC. Aircraft Inspection by Multirotor UAV Using Coverage Path Planning. *2021 International Conference on Unmanned Aircraft Systems (ICUAS).* 2021:575-581. doi: 10.1109/ICUAS51884.2021.9476718

46. Dai J, Gong X, Wang J. Coverage Path Planning Method of Unmanned Aerial Vehicle for Aircraft Surface Detection Task. *Journal of Mechanical Engineering.* 2023;59(16):243-253.
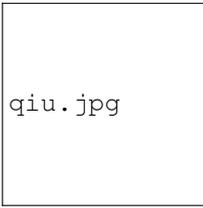
AUTHOR BIOGRAPHY

Yunlong Wang. Yunlong Wang was born in Rizhao, China, in 2000. He received the B.S. degree in mechanical engineering in 2022 from Xi'an Jiaotong University, Xi'an, China, where he is currently working toward the Ph.D. degree in mechanical engineering. His research interests include path planning of mobile robot and unmanned aerial vehicle.
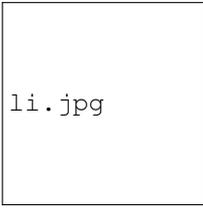
Shaoke Wan. Shaoke Wan was born in Xuchang, China, in 1990. He received the Ph.D. degree in mechanical engineering from Xi'an Jiaotong University, Xi'an, China, in 2019. He is currently an Associate Professor with Xi'an Jiaotong University. His research interests include the active vibration control, path planning of mobile robot, and intelligent manufacturing.

qiu.jpg

Rongcan Qiu. Rongcan Qiu was born in Longyan, China, in 2000. He received the B.S. degree in mechanical engineering in 2023 from Xi'an Jiaotong University, Xi'an, China, where he is currently working toward the M.S. degree in mechanical engineering. His research interests include path planning of mobile robot and unmanned aerial vehicle.

li.jpg

Xiaohu Li. Xiaohu Li was born in Pingxiang, China, in 1976. He received the Ph.D. degree in mechanical engineering from Xi'an Jiaotong University, Xi'an, China, in 2010. He is currently a Professor with Xi'an Jiaotong University. His research interests include path planning of mobile robot, unmanned aerial vehicle, and robot control.